Self Excited Half-Bridge Series Resonant Parallel Loaded Fluorescent Lamp Electronic Ballasts

T.-H. Yu, H.-M. Huang and T.-F. Wu

Power Electronics Applied Research Laboratory
Department of Electrical Engineering
National Chung Cheng University
Ming-Hsiung 62107, Chia-I, Taiwan, R.O.C.
Tel:886-5-2720411 Ext.6346; Fax:886-5-2720862

Abstract - **Time-domain analyses are given for the electronic ballasts adapted from a self excited half-bridge series resonant parallel loaded inverter operating in either high quality factor (>2.5) or low quality factor (≈1.0) conditions. The operational principles of the inverter applied as an electronic ballast are described in detail from which the voltage and current stresses imposed on switching devices can be determined analytically, and a systematic design procedure can be, therefore, outlined. In addition, practical considerations taking into account the storage time of the switching devices and the nonlinear characteristics of the saturable core are addressed. The computer simulations and experimental results from a laboratorial prototype are used to verify the theoretical predictions and discussions.**

I. Introduction

A great attention has been paid recently in the technology of designing and developing fluorescent lamp electronic ballasts, because numerous benefits can be obtained by high frequency operation of the lamps. At high frequency operation, luminous efficacy of fluorescent lamps is 10-20% higher than that of 60 Hz [1], flickers fall to unnoticeable levels, and annoying humming as well as stroboscopic effects can be omitted completely [1-7]. The size and weight of the inductors and capacitors used for current limiting in the high frequency operated electronic ballasts are much smaller than those in the traditional electro-magnetic ballasts. In addition, by implementing intelligent control scheme to the electronic ballasts, more energy saving from the lighting systems can be achieved. There are many resonant inverters that can serve as power stages of fluorescent lamp drivers. The self excited half-bridge series resonant parallel loaded inverter is one of the most popular topologies and has been developed into commercial electronic ballasts. In recent years, several papers have been published and dedicated in analyzing the series resonant parallel loaded electronic ballasts using fundamental approximation [8-10]. However, variations of the switching period due to the storage time of the BJT switches and the nonlinear characteristics of the saturable core have not yet been analytically addressed. In particular, these variations become more critical for the electronic ballasts with low quality factors in which the predescribed two effects primarily determine the switching frequency.

This paper presents steady-state analyses of the self excited half-bridge series resonant parallel loaded electronic ballasts taking into account the storage time and the effect of the saturable core. The system state equations and operating constraints are first listed and manipulated from which sets of control curves, groups of design rules, and steps of design procedures will be then illustrated and addressed analytically or numerically. Though the quantitative analyses in time-domain are complicated and troublesome, they yield accurate results when analyzing low Q systems. In practice, power switches are non-ideal. Particularly, it is worth pointing out that the storage time of the BJT is undesired long in typical applications and play important roles in determining switching period. Including the storage time in the analyses will make the paper become more uniquely valuable.

II. Operational Principle of the Electronic Ballast

A simplified schematic of the electronic ballast adapted from the described self excited series resonant parallel loaded inverter is shown in Fig. 1. The key components of this circuit are a series resonant tank (Cr,Lr), two pairs of alternatively driven switches, and three mutually coupled windings T1_1, T1_2 and T1_3 which are employed for driving switches Q1 and Q2. Each pair of switches consist of a transistor Q1(Q2) and an anti-parallel diode D1(D2). Switching devices Q1, Q2, D1 and D2 take turns conducting to form a switching cycle. It should be pointed out that with or without D1 and D2, the storage times of transistors vary widely resulting in different behaviors of systems.

After power is applied to the circuit shown in Fig. 1, the trigger which is formed by resistor R1 and capacitor C1 along with the DIAC initiates the self-excited processes; that is, the DIAC triggers transistor Q2 and then the system will run by itself. As C1 is charged upto the breakdown voltage of the DIAC, the DIAC conducts and a voltage pulse supplies to the base of Q2, thus turning it on immediately. This causes a current flowing through Cr, Lr, T1_1 and Q2, and inducing a positive voltage on winding T1_2. The induced voltage takes over

0-7803-2482-X/95 $4.00

the role of the trigger and drives Q2 into deep saturation while keeps Q1 off with a negative voltage induced on T1_3. Once switch Q2 is continuously turned on, the circuit establishes a resonant current in inductor Lr and through the primary winding T1_1. This varing current induces a change of magnetic flux density in the saturable core T1. When the current drives the core into a saturation region, the voltage induced on T1_2 drops to zero and the minority carriers stored in the base of Q2 are drained out. The duration from beginning to discharge the minority carriers until the transistor being turned off is defined as the storage time of Q2. At the moment that Q2 is turned off, it completes the half-period operation; therefore, the switching frequency f_s can be determined and, in addition, it can be shown that f_s is higher than the resonant frequency f_r. Typical current and voltage waveforms are depicted in Fig. 2(a) and 2(b). It should be noted that the storage time ($T_s/2 - t_i'$) lasts for around two-thirds of one-half switching period $T_s/2$. Once switch Q2 is truned off, the current flowing in Lr freely wheels through D1 and during this time interval, switch Q1 is turned on. Hence, transistor Q1 is turned on at zero voltage which results in eliminating trun-on switching losses. However, this circuit has significant switching losses during the trun-off transition. Usually, therefore, a lossless snubber capacitor (CQ1) is supplemented in parallel with Q1 to reduce turn-off switching losses to a negligible level. This phenomenon can be illustrated by Fig. 3 in which the cross over area of collector current i_c and collector-emitter voltage v_{ce} in Fig. 3(b) is much smaller than that in Fig. 3(a).

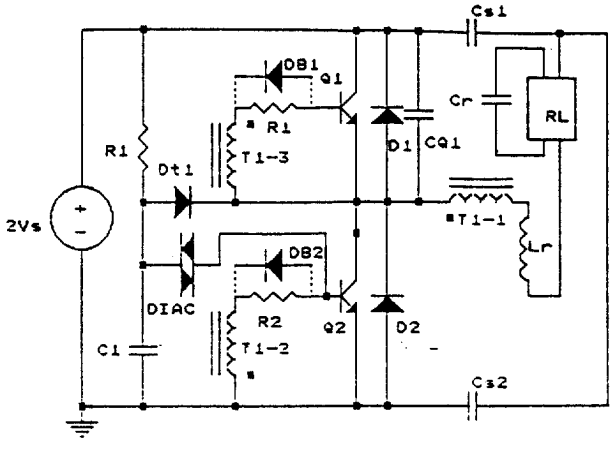

Fig. 1 Schematic of the self excited half-bridge series resonant parallel loaded electronic ballast.

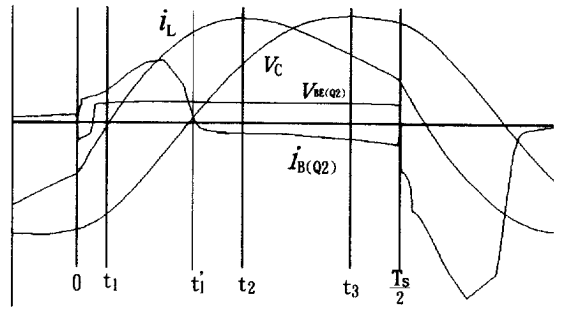

Fig. 2 The inductor current, capacitor voltage, base driving voltage and current waveforms.

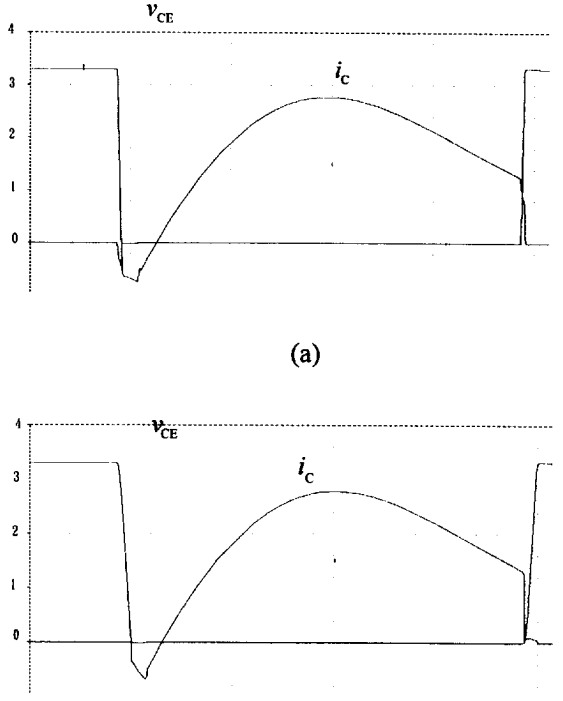

Fig. 3 Collector current and collector-emitter voltage waveforms of the circuit operated (a) without lossless snubber capacitor (CQ1) and (b) with the capacitor (CQ1).

III. Analyses of the Series Resonant Parallel Loaded Inverter

The series resonant parallel loaded inverter is the kernel of the proposed electronic ballast. To yield useful design information, theoretical analyses of such an inverter become essentially critical. For without losing the primary goal and purpose of writing this paper, we make the following reasonable assumptions in the analyses:

(1) The on-resistance of each switch is neglected.

(2) The effects of the lossless snubber are neglected.

(3) The arc voltage of the fluorescent lamp is much higher than those across the filaments so that the resistances of the filaments are negligible.
(4) Capacitance Cs1 >> Cr and Cs2 >> Cr.
(5) The power factor of the fluorescent lamp operated at high frequency is unity; that is, the equivalent impedance of the lamp is pure resistance.

In the following, we will derive the equivalent circuit from which the important parameters and equations can be determined

III.1 The Equivalent Circuit

According to the operational principles and assumptions metioned above, the schematic depicted in Fig. 1 can be further simplified and shown in Fig. 4. In the figure, usually, because of Cs1 >> Cr and due to the switching actions, the dc source can be replaced by a square wave voltage one. That is, voltage ripples on Cs1 and Cs2 during a switching period can be neglected. The amplitude of the square wave voltage source is Vs, where Vs = 1/2Vin. Since at high frequency operation a fluorescent lamp can be approximated by a resistor [1], the circuit becomes a second order low-pass filter. The parameters of the equivalent circuit can be summarized as follows: Resonant inductor $L = L_r$, resonant capacitor $C = C_r$ and $R = R_L$ represents the equivalent resistance of the lamp. The natural frequency ω_0, resonant frequency ω_r and damped frequency ω_d are defined by $\omega_0 = 1/\sqrt{LC}$, $\omega_r = \omega_0\sqrt{1-1/Q^2}$ and $\omega_d = \omega_0\sqrt{1-1/(4Q^2)}$, respectively. The angular switching frequency is denoted by $\omega_s = 2\pi f_s$; that is, the switching period $T_s = \frac{1}{f_s} = \frac{2\pi}{\omega_s}$. In addition, the characteristic impedance Z_0, the quality factor Q and damping factor α are denoted by $Z_0 = \sqrt{L/C}$, $Q = R/Z_0$ and $\alpha = 1/2RC$, respectively.

III.2 Analyses of the Circuit

In order to determine the component values, the dynamics of the equivalent network needs to be investigated, and from which several time moments are calculated so as the component ratings can be specified. For the equivalent circuit shown in Fig. 4, the state variable equations describing the dynamics of the network can be expressed as follows :

$$\dot{\underline{x}} = A\underline{x} + Bu \tag{1}$$

where vector $\underline{x}$ denotes the system states, A and B are constant matrices, and u is an input. Inductor current $i_L(t)$ and capacitor voltage $v_C(t)$ are chosen as state variables. Equation (1) can be rewritten and represented by the following equation sets:

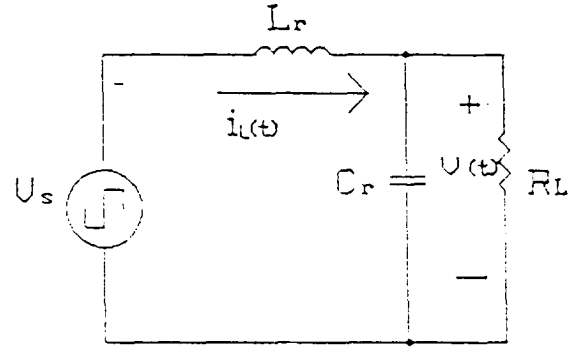

Fig. 4 A simplified equivalent circuit of that shown in Fig. 1.

$$\frac{d}{dt}\begin{bmatrix} i_L(t) \\ v_c(t) \end{bmatrix} = \begin{bmatrix} 0 & -1/L \\ 1/C & -1/RC \end{bmatrix}\begin{bmatrix} i_L(t) \\ v_c(t) \end{bmatrix} + \begin{bmatrix} 1/L \\ 0 \end{bmatrix} V_s \tag{2}$$

The general solutions of (2) are given as follows:

$$\begin{aligned} i_L(t) &= e^{-\alpha t}(-K_1\cos\omega_d t + K_2\sin\omega_d t) + \frac{V_s}{R} \\ &= K_3 e^{-\alpha t}\sin(\omega_d t - \theta_1) + \frac{V_s}{R} \quad , \quad 0 \le t \le \frac{T_s}{2} \end{aligned} \tag{3}$$

and

$$\begin{aligned} v_c(t) &= V_s + K_3 Z_0 e^{-\alpha t}\sin(\omega_d t - \theta_1 - \theta_2) \\ &= V_s + K_3 Z_0 e^{-\alpha t}\sin(\omega_d t - \theta_3) \quad , \quad 0 \le t \le \frac{T_s}{2} \end{aligned} \tag{4}$$

where

$$K_1 = I_{L0} + \frac{V_s}{R}, \quad K_2 = \frac{(I_{L0} - \frac{V_s}{R})e^{\alpha T_s/2} + K_1\cos\frac{\omega_d T_s}{2}}{\sin\frac{\omega_d T_s}{2}},$$

$$K_3 = (K_1^2 + K_2^2)^{1/2}, \quad \theta_1 = \tan^{-1}(\frac{K_1}{K_2}),$$

$$\theta_2 = \tan^{-1}(\frac{\omega_d}{\alpha}) = \tan^{-1}(\sqrt{4Q^2-1}),$$

$\theta_3 = \theta_1 + \theta_2$ *and*, $I_{L0} = -i_L(0)$.

At the steady state, there exist the following relationships:

$$i_L(0) = -i_L(\frac{T_s}{2}) = -I_{L0}, \tag{5}$$

and

$$v_c(0) = -v_c(\frac{T_s}{2}) = -V_{c0}. \tag{6}$$

Using the relationships shown in (5) and (6), I_{L0} and V_{C0} can be derived and shown as follows:

$$I_{L0} = \frac{(C_1B_2 - C_2B_1)}{(A_1B_2 - A_2B_1)} \tag{7}$$

and

$$V_{c0} = \frac{A_1C_2 - A_2C_1}{A_1B_2 - A_2B_1}, \quad (8)$$

where

$A_1 = L(\alpha + J\omega_d)$, $B_1 = -1$, $C_1 = V_s - L(\alpha + K\omega_d)\frac{V_s}{R}$,

$A_2 = (\alpha + J\omega_d)$, $B_2 = e^{\frac{\alpha T_s}{2}} \Big/ L$,

$C_2 = \frac{V_s}{L}e^{\frac{\alpha T_s}{2}} - (\frac{V_s}{R})[(\alpha + \omega_d K)\cos\frac{\omega_d T_s}{2} + (\omega_d - \alpha K)\sin\frac{\omega_d T_s}{2}]$,

$J = \frac{e^{\frac{\alpha T_s}{2}} + \cos\frac{\omega_d T_s}{2}}{\sin\frac{\omega_d T_s}{2}}$ and $K = \frac{\cos\frac{\omega_d T_s}{2} - e^{\frac{\alpha T_s}{2}}}{\sin\frac{\omega_d T_s}{2}}$.

Thus, (3) and (4) can be determined and represented in terms of parameters defined above.

There are several time moments which should be calculated for determining the component ratings. These include the time of t_1, t_2 and t_3 which satisfy the following relationships:

$i_L(t_1) = 0$, $\frac{di_L(t_2)}{dt} = 0$ and $\frac{dv_c(t_3)}{dt} = 0$,. It is explicit that the calculations of t_1, t_2 and t_3 can help to determine the diode current, capacitor voltage and inductor current ratings. Time t_2 and t_3 can be obtained readily, while t_1 needs to be solved using numerical method because $i_L(t_1)$ is a transcendental function. The expressions for t_2 and t_3 are shown following:

$$t_2 = \frac{\theta_3}{\omega_d}, \quad (9)$$

$$t_3 = \frac{1}{\omega_d}(\theta_1 + 2\theta_2), \quad (10)$$

Since the steady state solutions for $i_L(t)$ as well as $v_c(t)$, and the critical time moments have been obtained, we can utilize them when determining the component ratings. For simplicity, we define the following expressions:

$M_1(t) = -\frac{1}{\alpha} + \frac{\alpha}{\omega_0^2}\cos[2(\omega_d t - \theta_1)] - \frac{\omega_d}{\omega_0^2}\sin[2(\omega_d t - \theta_1)]$,

$M_2(t) = \omega_d\cos(\omega_d t - \theta_1) + \alpha\sin(\omega_d t - \theta_1)$,

$M_3(t) = -\frac{1}{\alpha} + \frac{\alpha}{\omega_0^2}\cos[2(\omega_d t - \theta_3)] - \frac{\omega_d}{\omega_0^2}\sin[2(\omega_d t - \theta_3)]$,

$M_4(t) = \omega_d\cos(\omega_d t - \theta_3) + \alpha\sin(\omega_d t - \theta_3)$,

$I_{LSI}(t) = \int i_L^2(t)dt$

$= \frac{1}{4}K_3^2 e^{-2\alpha t}M_1(t) - 2K_3\frac{V_S}{R}\frac{1}{\omega_0^2}e^{-\alpha t}M_2(t) + \frac{V_S^2}{R^2}t$,

$V_{CSI}(t) = \int V_C^2(t)dt$

$= \frac{1}{4}K_3^2 Z_0^2 e^{-2\alpha t}M_3(t) - 2V_S K_3 Z_0\frac{1}{\omega_0^2}e^{-\alpha t}M_4(t) + V_S^2 t$,

$V_{LSI}(t) = \int v_L^2(t)dt = \frac{1}{4}K_3^2 Z_0^2 e^{-\alpha t}M_3(t)$,

$I_{CSI}(t) = \int i_C^2(t)dt = -K_3 e^{-\alpha t}M_2(t) + \frac{K_3}{Q}e^{-\alpha t}M_4(t)$, *and*

$I_{LI}(t) = \frac{-K_3 e^{-\alpha t}}{\omega_0^2}M_2(t) + \frac{V_S}{R}t$.

The currents and voltages flowing through devices or across them can be then determined in terms of the above defined symbols.

R.M.S. inductor current:

$$I_{Lr} = \left[\frac{2}{T_s}\int_0^{T_s/2} i_L^2(t)dt\right]^{1/2} = \left\{\frac{2}{T_s}\left[I_{LSI}(\frac{T_s}{2}) - I_{LSI}(0)\right]\right\}^{1/2} \quad (11)$$

Peak inductor current:

$$I_{Lp} = i_L(t_2) = K_3 e^{\frac{-\alpha\theta_3}{\omega_d}}\sin\theta_2 + \frac{V_S}{R} \quad (12)$$

Peak switch current:

$$I_{SWp} = I_{L_p} = K_3 e^{\frac{-\alpha\theta_3}{\omega_d}}\sin\theta_2 + \frac{V_S}{R} \quad (13)$$

Peak diode current:

$$I_{Dp} = |i_L(0)| = I_{L_0} = \frac{C_1B_2 - C_2B_1}{A_1B_2 - A_2B_1} \quad (14)$$

R.M.S. capacitor voltage:

$$V_{Cr} = \left[\frac{2}{T_s}\int_0^{T_s/2} v_C^2(t)dt\right]^{1/2} = \left\{\frac{2}{T_s}\left[V_{CSI}(\frac{T_s}{2}) - V_{CSI}(0)\right]\right\}^{1/2} \quad (15)$$

Peak capacitor voltage:

$$V_{Cp} = v_c(t_3) = V_S + K_3 Z_0 e^{\frac{-\alpha(\theta_1+2\theta_2)}{\omega_d}}\sin\theta_2 \quad (16)$$

III.3 Normalization

In order to readily and widely apply the derived results in the design of the proposed ballasts, we introduce a per unit (p.u) system which is defined as follows:

$1p.u[V] = V_s = V_{base}$, $1p.u[Z] = R_{Arc} = Z_{base}$,

$1p.u[A] = V_{base}/Z_{base}$, $1p.u[\omega] = \omega_0 = \omega_{base}$,

$1p.u[T] = \frac{2\pi}{\omega_0} = T_{base}$, $1p.u[L] = Z_{base}/\omega_{base}$, *and*

$1p.u[C] = \frac{1}{(\omega_{base}\cdot Z_{base})}$.

Based on the per unit system, the graphs which are useful for designing the ballast are depicted and discussed in the following section. The procedure of determining the key component values is, therefore, established.

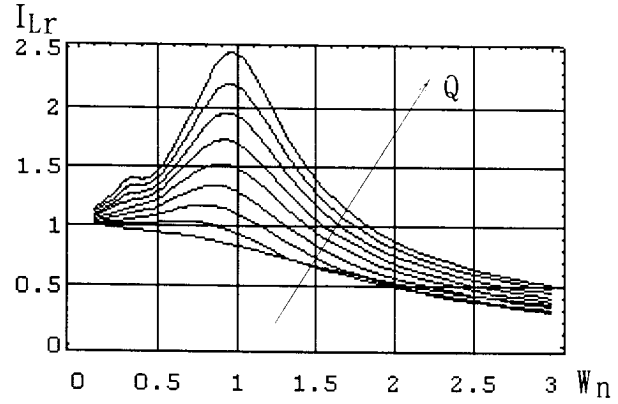

(a)

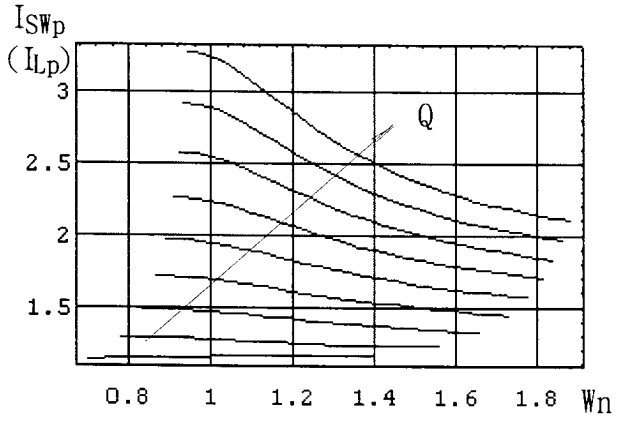

(b)

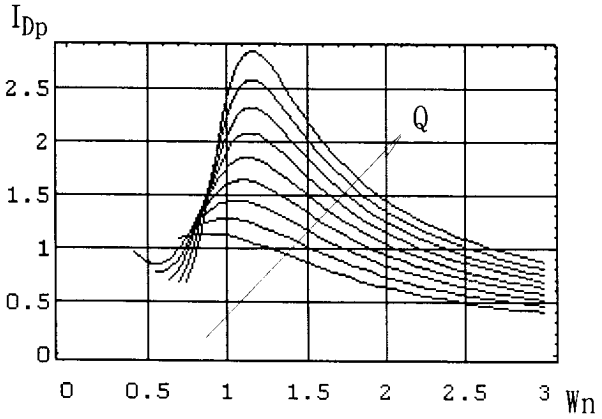

(c)

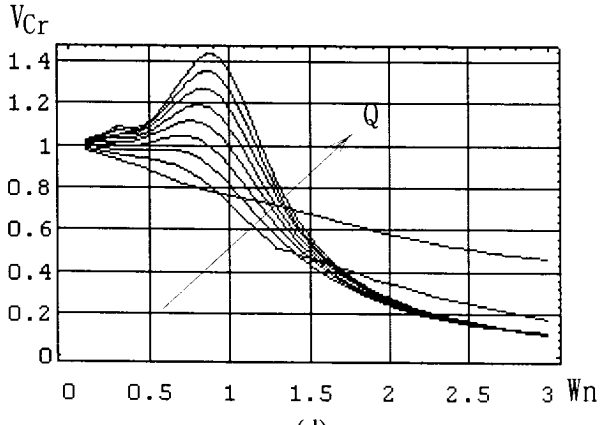

(d)

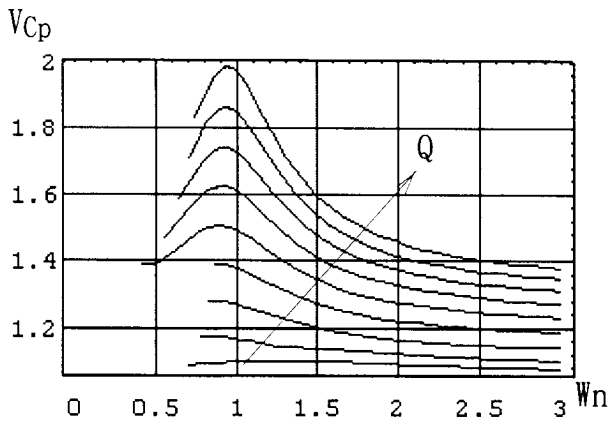

(e)

Fig. 5 Design curves for the design of the series resonant parallel loaded electronic ballast. (Q: 0.72, 0.8~1.5)

IV. Design Procedure

IV.1 Creation of Design Graphs

In designing the proposed electronic ballast, the given parameters include only the input voltage V_{in}, the specification of a lamp such as arc voltage V_{Arc} and arc current I_{Arc}, and the switching frequency. Except the pre-mentioned parameters, all the parameters are unknown and have to be calculated or determined by another methods. Since graphs present more useful and explicit information than equations do in designing a resonant inverter, the results of V_{cr}, I_{Lr}, I_{Lp}, V_{cp}, I_{swp} and I_{Dp} obtained in section III.2 are plotted in Figs. 5(a)-5(e) as functions of normalized switching frequency. These graphs will be utilized in determining the component values. The detail is shown in the following sub-section.

IV.2 Determination of Component Values

In order to make use of the analytic results derived previously, the specified parameters (V_{Arc}, R_{Arc} and ω_s) are first normalized to its corresponding base, and the component values are then determined using graphic approximation method. The normalized parameters are collected as follows:

$$V_{Arc(n)} = \frac{V_{Arc}}{V_{base}} = \frac{V_{Arc}}{V_s} \qquad p.u[V] \tag{17}$$

$$R_{Arc(n)} = 1 \qquad p.u[Z] \tag{18}$$

$$I_{Arc(n)} = \frac{V_{Arc(n)}}{R_{Arc(n)}} = V_{Arc(n)} \qquad p.u[A] \tag{19}$$

$$\omega_n = \frac{\omega_s}{\omega_0} \tag{20}$$

In the above parameters, ω_0 is exclusively unknown.

(1)Determining the Q and ω_0

As can be seen from Fig. 5(d), the rms value of capacitor voltage $V_C(t)$ is quite dependent on the quality factor Q and the ω_n. In the figure there are many choices of Q and ω_n which meet the requirement of $V_{Cr} = V_{Arc(n)}$.

Usually, a lower Q is chosen so as the component stresses of the switches, the resonant inductor and capacitor can be reduced. Also, a lower Q system possesses the property of low sensitivity but might yield high current crest factor. If Q is determined to be Q1, one can read $\omega_n = \omega_{n1}$ from Fig 5(d). Thus, the natural frequency ω_{01} can be calculated using the following equation:

$$\omega_{01} = \frac{\omega_s}{\omega_{n1}} \tag{21}$$

(2) Calculating the resonant component values.

Once the ω_0 and Q are determined, the resonant inductor and capacitor can be calculated using the following relationships:

$$\frac{1}{\sqrt{L_r C_r}} = \omega_{01} \tag{22}$$

and

$$\frac{R_{Arc(n)}}{\sqrt{L_r/C_r}} = \frac{1}{\sqrt{L_r/C_r}} = Q_1 . \tag{23}$$

(3) Construction of the switching period.

The resonant devices can be determined primarily due to that the self-excited switching period is specified and treated as a constant value. However, there are many variables such as the specifications of the saturable core and the power bipolar junction transistor (BJT) which are highly related to the switching period. It can be observed that the switching period comprises two main time intervals: (a) the time interval of the core operated in non-saturation region, and (b) the time interval during the storage time of a power BJT. Thus, the selection of a power BJT as well as the design of its base driver, and the choice of a saturable core become relatively critical when constructing the switching period. A detailed description in determining these values is presented as follows:

For convenience, the base driving circuit is redrawn and shown in Fig. 6(a), of which its associated waveforms are depicted in Fig. 6(b). Fig. 6(c) illustrates the B-H curve for the saturable core operating in the circuit. The interested two time intervals are: Interval 1: core - non-saturation interval (0-t_4) and Interval 2 : storage time (t_4-$\frac{T_s}{2}$).

(a) Determination of t_4

From the waveforms shown in Fig. 6(b), it can be seen that the base current i_{T_2} is zero at the time t = t_4, thus, we can obtain the following relationship:

$$i_L(t_4) = I_{L(SAT)}, \tag{24}$$

where $I_{L(SAT)}$ is the current that flows through the primary winding of the base driving transformer and drives the core into its saturation region. Inductor current $I_{L(SAT)}$ is determined by characteristics of the core and the number of turns winded on it. In the design, we first specify the t_4; that is, $I_{L(SAT)}$ is fixed, and then find an appropriate combination of a core and a number of turns which can yield this $I_{L(SAT)}$.

According to (3) and (24), t_4 can be determined from the following equation:

$$e^{-\alpha t} \sin(\omega_d t_4 - \theta_1) = \frac{1}{K_3}\left(I_{L(SAT)} - \frac{V_s}{R}\right) \tag{25}$$

(b) Selection of the power BJT and its base resistor R_b

As described previously, the switching period comprises two primary time intervals. Hence, once t_4 is determined, the storage time t_s can be represented by the following equation:

$$t_s = \frac{T_s}{2} - t_4 . \tag{26}$$

The storage time t_s of a power BJT, however, is a complicated function of the forward base current I_{bf}, the reversed base current I_{br}, the current gain β in the saturation mode, the collector current I_c and the minority carrier life time τ_e in the base, and is represented in equation (27) [11].

$$t_s = \tau_e \ell n\left(\frac{n+1}{n+I_c/\beta I_{bf}}\right) \tag{27}$$

where $n = \frac{I_{br}}{I_{bf}}$. In our case, I_{bf} is not constant at all. Thus, for simplicity but without losing the accuracy, I_{bf} is replaced by its averaged value $\bar{I}_{bf}$ which equals to $\bar{V}_{T\_2}/R_b$, where $\bar{V}_{T\_2}$ represents the averaged value over the time interval of 0 to t_4. Moreover, the collector current is approximated to be I_{Cr}. The life time τ_e and the current gain β can be obtained from a simple testing circuit, which can be, usually, found in a power BJT data book. As a summary, R_b can be determined from the following simultaneous equations:

$$t_s = \frac{T_s}{2} - t_4 = \tau_e \ln\left[\frac{\bar{V}_{T\_2}}{V_{BE(sat)} + \frac{R_b I_{Cr}}{\beta}}\right], \tag{28}$$

$$i_{T\_1} = i_L - (\frac{v_{T\_2} - V_{BE(sat)}}{R_b} * \frac{N_2}{N_1}), \quad (29)$$

$$L_{T\_1}\frac{di_{T\_1}}{dt} = \frac{N_1}{N_2} v_{T\_2}, \quad (30)$$

$$\overline{V}_{T\_2} = \frac{1}{t_4}\int_0^{t4} v_{T\_2} dt, \quad (31)$$

where N_1 and N_2 are the number of turns of the primary winding and the secondary winding of the driving transformer, respectively.

It is very troublesome to solve for R_b directly from (28) to (31). The suggested approach to determine R_b is using a computer simulation. For instance, using the .STEP function in SPICE program running recursively and iterately can finally yield a proper R_b to satisfy the above equations [12].

(4)Determination of Component ratings

To complete the selection of components in the design, their current and voltage ratings need to be specified. Fig. 5(a)~ 5(e) illustrate the ratings of several key components. For example, given a Q and an ω_n, the peak current I_{swp} flowing through the switches can be read out from Fig. 5(b). In addition, it can be observed that the peak current or voltage varies widely with the changes of ω_n.

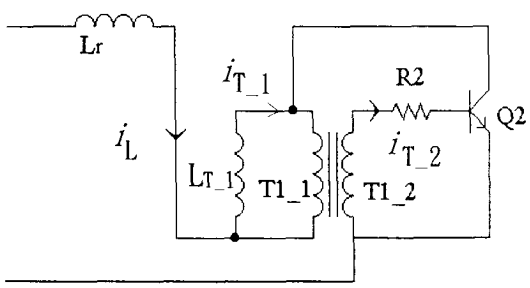

(a)

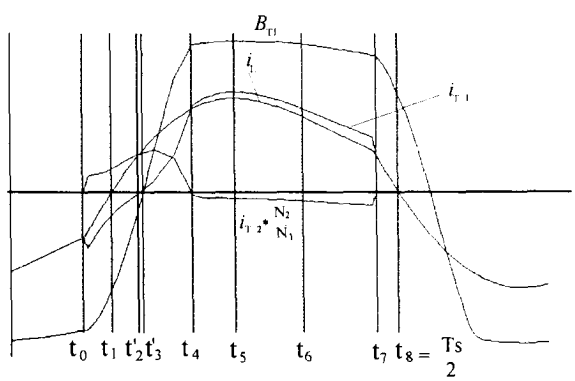

(b)

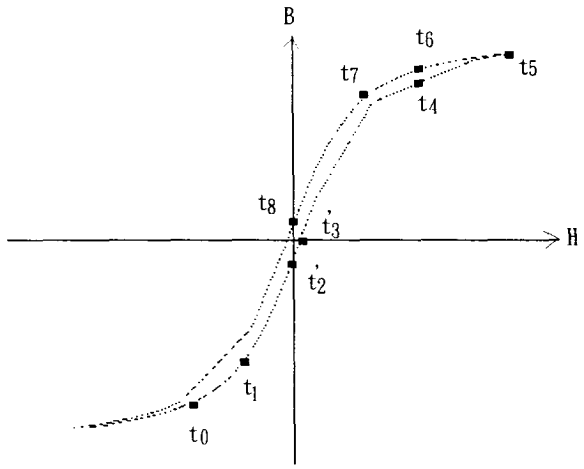

(c)

Fig. 6 (a) The base driving circuit of the schematic shown in Fig. 1 for determining the core-non-saturation interval.
(b) The related current and voltage waveforms of the circuit shown in 6(a).
(c) The B-H curve for the saturable core operating in the circuit shown in 6(a).

V. Computer Simulation and Experimental Results

To illustrate the design procedure, a laboratorial electronic ballast is implemented, where its design parameters are listed as follows :

$V_{in} = 2V_s = 160V$, $C_{S1} = C_{S2} = 1uF$,
$C_r = 18nF$, $L_r = 2.5mH$,
$R_b = 22ohm$, *and* $f_s = 25KHz$.

The fluorescent lamp used in the design example is a Two-D 38 watt lamp whose specifications are

$V_{Arc} = 120V_{(rms)}$, $I_{Arc} = 300mA_{(rms)}$, *and* $R_{Arc} = 400ohm$.

Fig. 7(a) and 7(b) shows the waveforms of the arc voltage and current of the lamp, yielded from the simulated and experimental results. They are found that the results are highly consistant except at the peak of the current. It is worth pointing out that the determination of a proper storage time takes a lot of efforts because this parameter (can be considered as a coersive parameter) varies with any change of most of the BJT parameters and temperature. For an engineer's approach, circuit simulators are helpful when determining this parameter used in the design.

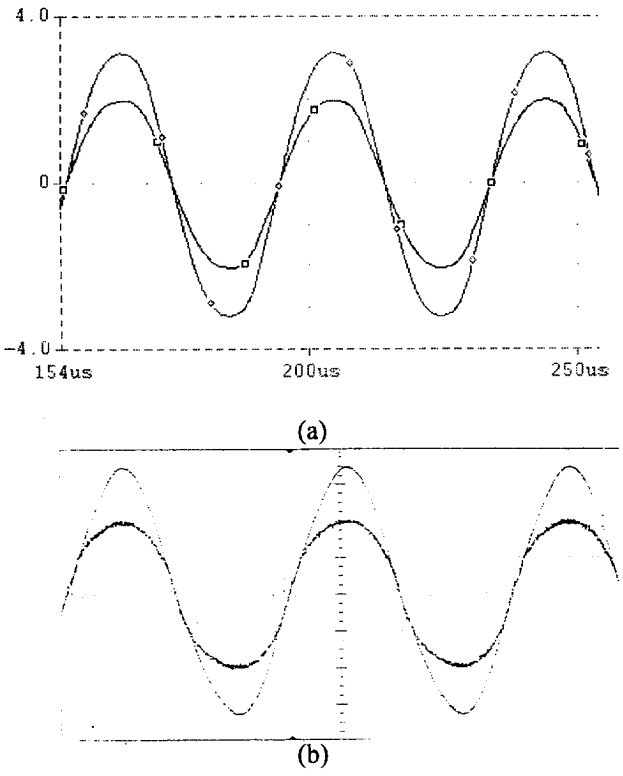

Fig. 7 (a) Simulated waveforms for the arc voltage and current of the lamp.
(b) Experimental waveforms for the arc voltage and current of the lamp.

VI. Conclusion

In this paper, a self-excited half-bridge series resonant parallel loaded electronic ballast has been analyzed in detail. The closed form solutions for $i_L(t)$ and $v_C(t)$ are derived, on which the normalized design curves used for selecting the component values and ratings are illustrated, thus simplifying the design procedure as well. Based on a time domain analysis and supported by computer simulators, a systematic design procedure has been outlined. To demonstrate the design procedures, and verify the analytic results, a prototype of the electronic ballast is implemented.

There exist some discrepancies between the the predicted and the measured results, due to the assumption of modeling the fluorescent lamp as a resistor. For further improvement of the consistency, modeling the fluorescent lamp more accurate are indispensable.

References

[1] E. E. Hammer, "High Frequency Characteristics of Fluorescent Lamps up to 500 kHz, " *Journal of the IES*, winter, 1987, pp.52-61.

[2] K. H. Jee, E. C. Nho and G. H. Cho, "High Frequency Resonant Inverter for Group Dimming Control of Fluorescent Lamp Lighting Systems, " *Journal of the IES*, 1989, pp.149-154.

[3] M. Jordan and J. A. O'Connor, "Resonant Fluorescent Lamp Conveter Provides Efficient and Compact Solution, " Proceedings of APEC, San Diego, CA, Feb. 1993, pp.424-431.

[4] E. E. Hammer and T. K. McGowan, "A New Optimized Fluorescent Lamp and Ballast for Low-Energy General Lighting Applications, "*IEEE Trans. on Industry Applications*, Vol. IAS-19, No.4, July/Aug. 1983, pp.646-651.

[5] R. R. Verderber, O. C. Morse and F. M. Rubinstein, "Performance of Electronic Ballast and Controls with 34- and 40-Watt F40 Fluorescent Lamps, " *IEEE Trans. in Industry Applications*, Vol. 25,No. 6, Nov./Dec. 1989, pp. 1049-1059.

[6] J. R. Kinsley, "Understanding the Use of New Fluorescent Ballasts Designs, " *EC&M*, Mar. 1990, pp.67-73.

[7] T.-H. Yu, L.-M. Wu and T.-F. Wu, "Comparisons Among Self-Excited Parallel Resonant, Series Resonant and Current-Fed Push-Pull Electronic Ballasts, " Proceedings of APEC' 94, Orlando, FL, pp.421-426.

[8] N. Mohan, T. M. Undeland and W. P. Robbins, Power Electronics: Converters, Applications and Design, John Wiley and Sons, 1987.

[9] M. K. Kazimierczuk and W. Szaraniec, "Electronic Ballast for Fluorescent Lamps, " *IEEE Trans. on Power Electronics*, Vol. 8, No. 4, pp.386-395, Oct. 1993.

[10] M. C. Cosby and R. M. Nelms, "Designing a Parallel-Loaded Resonant Inverter for an Electronic Ballast Using the Fundamental Approximation, " Proceedings of APEC' 93, San Diego, CA, pp.418-423.

[11] B. W. Williams, Power Electronics: Devices, Drivers, Applications and Passive Components, McGraw - Hill, Inc. 1992.

[12] Y. Sun, "PSpice Modeling of Electronically Ballasted Compact Fluorescent Lamp Systems, " Proceedings of IAS'93, pp.2311-2316.